

JGR Space Physics

,

RESEARCH ARTICLE

10.1029/2025JA034329

Key Points:

- Multiple satellites and ground observations enabled the first definitive identification of the inner radial boundary of a substorm injection
- The first coincident observation of a localized electron injection and corresponding hiss wave generation
- Identification of the substorm injection and slot-filling as two spatially and temporally distinct events

Supporting Information:

Supporting Information may be found in the online version of this article.

Correspondence to:

G. D. Reeves and J.-F. Ripoll, Geoff@ReevesResearch.org; Jean-Francois.Ripoll@cea.fr

Citation:

Reeves, G. D., Ripoll, J.-F., Blum, L. W., Cully, C. M., Colpitts, C. A., Cosmides, M., et al. (2025). Multi-platform observations of the radial penetration of substorm injected electrons and subsequent slot-filling event. *Journal of Geophysical Research: Space Physics*, 130, e2025JA034329. https://doi.org/10.1029/2025JA034329

Received 17 JUN 2025 Accepted 13 OCT 2025

Author Contributions:

Conceptualization: Jean-Francois Ripoll, Lauren W. Blum, Christopher M. Cully, Richard B. Horne, David M. Malaspina, Robyn M. Millan, Yoshizumi Miyoshi, Drew L. Turner, Hilde N. Nesse, Aleksandr Y. Ukhorskiy, Maria E. Usanova

Data curation: Christopher M. Cully, Reihaneh Ghaffari, Keisuke Hosokawa, Yoshi Kasahara, Satoshi Kurita, Takefumi Mitani, Viviane Pierrard, Shoichiro Yokota

© 2025. The Author(s).

This is an open access article under the terms of the Creative Commons
Attribution-NonCommercial-NoDerivs
License, which permits use and
distribution in any medium, provided the original work is properly cited, the use is non-commercial and no modifications or adaptations are made.

Multi-Platform Observations of the Radial Penetration of Substorm Injected Electrons and Subsequent Slot-Filling Event

Geoffrey D. Reeves^{1,2} , Jean-Francois Ripoll^{3,4} , Lauren W. Blum⁵ , Christopher M. Cully⁶ , Christopher A. Colpitts⁷ , Mélanie Cosmides³ , Sadie S. Elliot⁸ , Reihaneh Ghaffari⁶ , Ashley D. Greeley⁸ , Richard B. Horne⁹ , Keisuke Hosokawa¹⁰ , Allison N. Jaynes¹¹ , Yoshi Kasahara¹² , Satoshi Kasahara¹³ , Kunihiro Keika¹⁴ , Satoshi Kurita¹⁵ , David M. Malaspina⁵ , Adam T. Michael¹⁶ , Robyn M. Millan¹⁷ , Takefumi Mitani¹⁸ , Yoshizumi Miyoshi¹⁴ , Viviane Pierrard¹⁹ , Drew L. Turner¹⁶ , Hilde N. Nesse²⁰, Aleksandr Y. Ukhorskiy¹⁶ , Maria E. Usanova⁵ , Maria Voskresenskaya² , and Shoichiro Yokota²¹

¹Los Alamos National Laboratory, Los Alamos, NM, USA, ²The New Mexico Consortium, Los Alamos, NM, USA, ³CEA, DAM, DIF, Arpajon, France, ⁴Université Paris-Saclay, CEA, LMCE, Bruyères-le-Châtel, France, ⁵Laboratory for Atmospheric and Space Physics, University of Colorado, Boulder, CO, USA, ⁶Department of Physics and Astronomy, University of Calgary, Calgary, AB, Canada, ⁷School of Physics and Astronomy, University of Minnesota, Minneapolis, MN, USA, ⁸NASA Goddard Spaceflight Center, Greenbelt, MD, USA, ⁹British Antarctic Survey, Cambridge, UK, ¹⁰University of Electro-Communications, Chofu, Japan, ¹¹Department of Physics and Astronomy, University of Iowa, Iowa City, IA, USA, ¹²Graduate School of Natural Science and Technology, Kanazawa University, Kanazawa, Japan, ¹³Research Institute for Sustainable Humanosphere, Kyoto University, Uji, Japan, ¹⁴Department of Earth and Planetary, Science, The University of Tokyo, Tokyo, Japan, ¹⁵Institute for Space-Earth Environmental Research, Nagoya University, Nagoya, Japan, ¹⁶The Johns Hopkins University Applied Physics Laboratory, Laurel, MD, USA, ¹⁷Department of Physics and Astronomy, Dartmouth College, Dartmouth, NH, USA, ¹⁸Institute of Space and Astronautical Science, Japan Aerospace Exploration Agency, Sagamihara, Japan, ¹⁹Université catholique de Louvain, Earth and Life Institute - Climate Sciences, Louvain-la-Neuve, Belgium, ²⁰Department of Physics and Technology, University of Bergen, Norway, ²¹The University of Osaka, Osaka, Japan

Abstract On 15 February 2018 a co-rotating interaction region (CIR) from an equatorial coronal hole reached the Earth. The CIR initiated a moderate and slowly intensifying geomagnetic storm, which began with a large and strong substorm injection. The substorm injection was exceptionally well-observed by an array of spacecraft including LANL-GEO satellites, Van Allen Probes (RBSP), Arase (ERG), and MetOp/POES, as well as ground-based instruments. These observations enable the unambiguous identification of several important features that have been impossible to measure directly in other events. The substorm injection extended well inside the geosynchronous orbit. A fortuitous conjunction of RBSP-A (moving inbound) and Arase (simultaneously moving outbound at the same magnetic local time) allows us to establish, very precisely, the location of the inner edge of the injection region at L = 3.8-3.9. In supporting observations, North American riometers saw precipitation extending down to $L \approx 4$ but not lower. Arase and RBSP-A also observed whistlermode hiss waves inside the plasmasphere. Analysis of the resonance conditions shows, conclusively, and for the first time, that they were produced by the drifting injected electrons. RBSP-A observations also show the injection (or transport) of electrons into or through the slot region within hours of the substorm injection onset. Previous studies were not able to clearly connect or separate substorm injections and slot-filling processes. These new observations clearly identify slot-filling as a spatially and temporally separate process that is not a direct result of substorm injection.

1. Introduction

On 15 February 2018, a strong auroral substorm (AE > 600 nT) marked the beginning of a moderate and slowly developing geomagnetic storm initiated by a co-rotating interaction region (CIR). CIRs (a.k.a., stream interaction regions, SIRs) are produced when high-speed solar wind streams (HSS) overtake the slower solar wind forming a compression region where the slow and fast streams are separated by a stream interface (e.g., Gosling et al., 2012). CIR/HSS-driven storms (e.g., Smith & Wolfe, 2012) and radiation belt enhancement events (e.g., Reeves, 1998)

REEVES ET AL. 1 of 16



Journal of Geophysical Research: Space Physics

10.1029/2025JA034329

Formal analysis: Jean-Francois Ripoll, Christopher M. Cully, Mélanie Cosmides, Sadie S. Elliot, Reihaneh Ghaffari, Ashley D. Greeley, Keisuke Hosokawa, Allison N. Jaynes, Yoshi Kasahara, David M. Malaspina, Adam T. Michael, Yoshizumi Miyoshi, Maria Voskresenskaya Funding acquisition: Jean-Francois Ripoll, Yoshizumi Miyoshi Investigation: Jean-Francois Ripoll, Christopher M. Cully, Mélanie Cosmides, Sadie S. Elliot, Ashley D. Greeley, Richard B. Horne, Allison N. Jaynes, Yoshi Kasahara, Kunihiro Keika, David M. Malaspina, Yoshizumi Miyoshi, Drew L. Turner, Maria Voskresenskaya Methodology: Jean-François Ripoll. Christopher M. Cully, Mélanie Cosmides, Sadie S. Elliot, Ashley D. Greeley, Allison N. Javnes, Yoshi Kasahara, David M. Malaspina, Yoshizumi Miyoshi, Drew L. Turner, Hilde N. Nesse, Aleksandr Y. Ukhorskiy, Maria E. Usanova, Maria Voskresenskava

Resources: Satoshi Kasahara, Satoshi Kurita

Software: Maria Voskresenskaya Supervision: Satoshi Kasahara Writing – original draft: Jean-Francois Ripoll, David M. Malaspina, Yoshizumi Miyoshi

Writing – review & editing: Jean-Francois Ripoll, Lauren W. Blum, Christopher M. Cully, Mélanie Cosmides, Sadie S. Elliot, Ashley D. Greeley, Keisuke Hosokawa, Allison N. Jaynes, Kunihiro Keika, David M. Malaspina, Adam T. Michael, Robyn M. Millan, Yoshizumi Miyoshi, Hilde N. Nesse, Maria E. Usanova, Maria Voskresenskaya often recur with a 27-day period primarily in the declining phase of the solar cycle. Properties of CME-driven and CIR-driven geomagnetic events are compared in an extended table in Borovsky and Denton (2006).

Geomagnetic storms typically (perhaps always) start with an auroral substorm and associated energetic particle injections but show ongoing activity for longer than isolated substorms (Reeves & Henderson, 2001). Substorm injections occur when energetic particles are transported, by dipolarizing magnetic flux tubes, from the plasma sheet to the closed drift paths of the inner magnetosphere (e.g., Mauk, 1986; Quinn & Southwood, 1982). Substorm injections are commonly observed at geosynchronous orbits where continuous measurements have been available since the 1970s. Starting with the NASA/USAF Combined Release and Radiation Effects Satellite and continuing through the NASA Van Allen Probes mission (a.k.a RBSP), studies have looked at the propagation of the injection region to L-shells inside geosynchronous orbit (Friedel et al., 1996; Motoba et al., 2020; Nosé et al., 2010; Reeves, Friedel, et al., 1996; Sergeev et al., 1998) where propagation speeds reduce dramatically from >100 km/s to tens of km/s (Malaspina et al., 2015; Reeves, Friedel, et al., 1996). It is widely assumed that the injections continue to slow and eventually stop as the magnetic field intensifies with decreasing radial distance. However, to date, no definitive measurements have been made of the minimum radial propagation distance: that is where any particular injection stops. Throughout this paper "L-shell" refers to the Roederer L* parameter (Roederer, 1967) calculated in the Olsen-Pfitzer quiet-time magnetic field model (Olson & Pfitzer, 1974). In a dipole magnetic field, the parameter L*, also known as the third adiabatic magnetic invariant, reduces to L, which is the radial distance (in Earth Radii) to the equator of any given field line.

"Injections" (or "transport") of energetic particles are also known to penetrate through the slot region and into the inner radiation belts. However, the physical mechanisms that produce these "slot-filling" or "slot-penetrating" events are not yet well-understood. In particular, to date, it has been impossible to determine if substorm injections and slot-filling transport occur simultaneously, together, or are spatially and/or temporally separated.

This article is organized as follows. Section 2 presents the event and the available multi-platform observations. Section 3 discusses the drifting electron injection signatures that reveal the minimum radial extent of the injection. Section 4 adds supporting observations of the electron precipitation measured on the ground and of the generation of hiss waves during the injection. Section 5 presents the electron transport in the slot region following the injection. Section 6 offers a summary of the results and the conclusions.

2. Event Description and Multi-Platform Observations

Figure 1 shows the period of interest on 15 February 2018, shaded in red. Moderate southward interplanetary magnetic field (IMF, $Bz \approx -8$ nT) produced a weak storm response (Sym-H > -20 nT) and moderate AE activity (≈ 600 nT) (Auroral observations are presented in Section S1 in Supporting Information S1). The event was embedded in a CIR (shaded in blue) generated from a high speed stream from a large equatorial coronal hole. The entire storm also included subsequent moderately fast high speed streams and Alfvénic solar wind fluctuations (shaded in green).

2.1. Satellite Locations and Foot Points

Satellites used in this study include geosynchronous satellites (LANL-GEO), the two Van Allen Probes satellites (RBSP A and B), the JAXA Arase satellite (a.k.a. ERG which is in an inclined geosynchronous transfer orbit, GTO), and several low-Earth Orbit (LEO) satellites (MetOp/POES and Proba V). Figure 2 shows the orbits in the equatorial and meridian planes of all satellites at GEO and GTO orbits used in this study: the LANL geostationary orbit satellites (01A, 02A, 04A, 97A) (e.g., Belian et al., 1996; Reeves, Belian, et al., 1996), RBSP A and B (Mauk et al., 2012), and Arase (Miyoshi, Hori, et al., 2018, Miyoshi, Shinohara, et al., 2018). Satellite positions are marked at 17:00 UT, just before the main injection was observed in geosynchronous orbit (Section 2.2). As shown in Figure 2, RBSP-A was inbound and Arase was outbound with both satellites located near $L \approx 4.5$ and MLT ≈ 9 .

The main period of interest for this study is from 16:30 UT to 18:00 UT. Figure 3 shows the magnetic foot points (3a), the MLT (3b) and *L*-shells (3c) of RBSP A and B, Arase, and MetOp 2. Figure 3a also shows the location of the ground riometers of the Geospace Observatory Riometer Network (GO-RIO). Ground observations will be discussed further in Section 4.1.

REEVES ET AL. 2 of 16

21699402, 2025, 11, Downloaded from https://agupubs.onlinelibrary.wiley.com/doi/10.1029/2025IA034329 by British Antarctic Survey, Wiley Online Library on [03/11/2025]. See the Terms and Condit

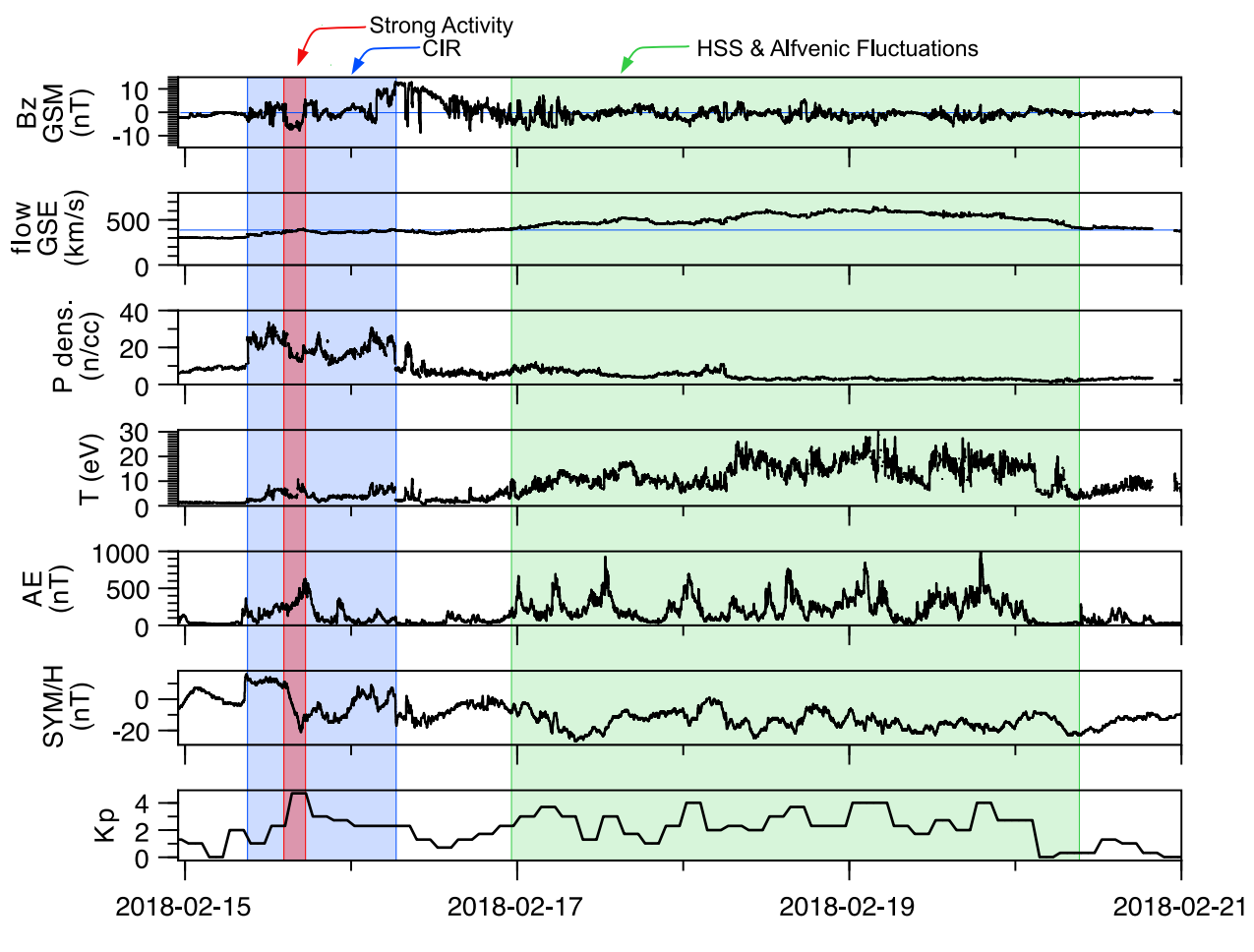


Figure 1. OMNI data from 14 February 2018 to 21 February 2018. From top to bottom: *z*-component of the Earth magnetic field (*Bz*), solar wind speed (flow, solar wind proton density (*P*)), solar wind temperature (*T*), the AE geomagnetic index, the Sym-H index, and the *Kp* index. All data except *Kp* have 1-min resolution (Papitashvili & King, 2020).

2.2. Geosynchronous Observations

Substorm injection activity was well-observed in geosynchronous orbit with four satellites distributed across the night side. Figure 4 shows 2 days of data from all four satellites. A sustained growth phase dropout was observed associated with a southward turning of the IMF Bz starting around 12:00 UT on February 15. Figure 5 shows a blow-up of the period from 15:00 to 18:00 for satellites LANL-04A and LANL-02A, which were located pre- and post-midnight respectively. Injection activity during this period was complex with multiple dispersed and dispersionless injections, which is typical of storm-time substorm activity (e.g., He et al., 2023; Reeves et al., 2003). (When fluxes at multiple energies simultaneously increase, the injection is referred to as "dispersionless" and indicates that the satellite is within the initial injection region. Following the dispersionless injection energetic particles gradient-curvature drift East (electrons) or West (ions) away from the injection region and are observed as an energy-dispersed signature.)

Several weak injections during the ongoing growth phase are observed and may be indicative of the so-called pseudo-breakup activity (e.g., Nakamura et al., 1994; Pulkkinen, 1996). Starting at ~16:44 UT there are a series of injections that gradually increase the fluxes at LANL-02A located in the night sector at 2 MLT. The injection activity is similar at LANL-04A located in the dusk-night sector at 21 MLT but occurs with different timings. The main injection is seen simultaneously by both satellites at 16:59:40 UT. Since the satellites were separated by 5 hr of MLT, we know that the azimuthal extent of the dispersionless injection region for this event is at least that wide, which again is fairly common for storm-time substorms (e.g., Henderson et al., 2006). While few substorms inject electrons with energies greater than ~300 keV (e.g., Friedel et al., 1996) this injection extended up to 800 keV as seen in the gold (bottom) curve in Figure 5a.

REEVES ET AL. 3 of 16



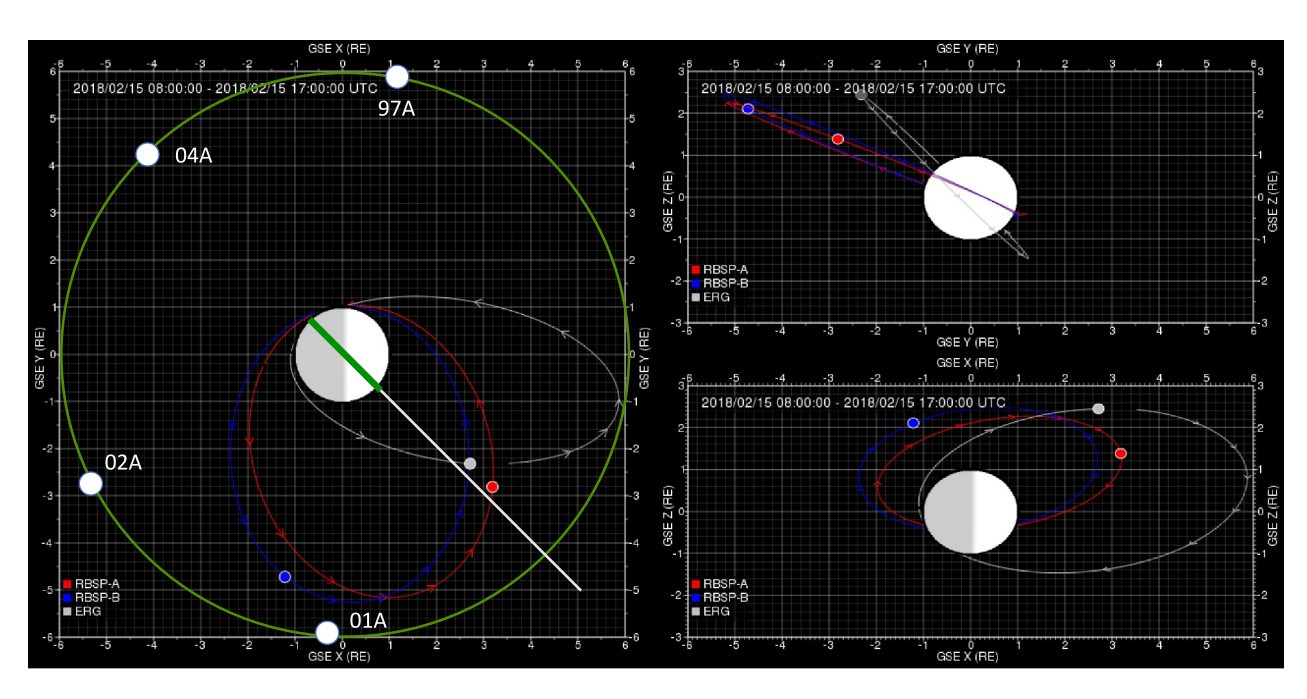


Figure 2. Multi-point satellite observations taken on 15 February 2018 at 17:00 UT in (a) the equatorial plane, (b) the meridional plane (perpendicular to the Sun-Earth axis), and (c) the meridional plane (on the Sun-Earth axis). Orbits of the LANL geosynchronous orbit satellites (01A, 02A, 04A, 97A), Van Allen Probes (red) A and (blue) B (noted RBSP A and B), and (white) Arase (noted ERG) are shown.

3. Drifting Electron Injection Signatures

After the dispersionless injection near midnight MLT, the electron gradient-curvature drifts eastward (toward dawn) with drift velocities that increase linearly with energy. Figure 6 compares the energy-dispersed drifting electron populations observed by Arase and the two RBSP satellites in both spectrogram and line-plot format.

Arase data are from the high-energy particle and medium-energy particle experiments; HEP (\sim 200–1,000 keV) and MEP-e (\sim 10–200 keV) (Kasahara et al., 2018; Mitani et al., 2018) and the Van Allen Probes data are from the Magnetic Ion-Electron (MagIES) spectrometer (Blake et al., 2013). The MagIES instrument is capable of direct measurement and subtraction of background from penetrating radiation such as inner belt protons, Bremsstrahlung, and galactic cosmic rays (Claudepierre et al., 2015). This background-subtracted data product is what is plotted in Figure 6. At L > 4 and energies below \sim 200 keV (where backgrounds are low compared to electron fluxes), MagIES uses a high-data-rate mode instead, so the background-corrected data in Figure 6c appear to have a gap. Continuous, non-background-corrected MagIES data are shown in Figure 11.

All three satellites were inside geosynchronous orbit (c.f. Figures 2 and 3). RBSP-B, near 5 MLT, observed the drifting electrons before RBSP-A and Arase and observed electrons both from the 16:59:40 UT injection and the weaker activity that preceded it. The main electron injection arrived at both Arase and RBSP-A satellites around 17:10 UT as seen in the highest energy channels with lower energies arriving later, as expected. As Arase moved outward from $L \sim 4.5$ to $L \sim 5.2$ (at $\sim 18:00$ UT), it continued to measure the injection, which was stronger at higher L-shells. RBSP-A, moving inbound, saw only a weak "wisp" at high energies, from ~ 200 to ~ 600 keV, which ended at $\sim 17:30$ UT when RBSP-A was at L = 3.8-3.9.

The combination of Arase and RBSP-A observations of the same injection is key to identifying L=3.8-3.9 as the inner edge of the injection region for this event. If injected electrons had been present below L<3.8, RBSP-A would have observed the continuation of the "wisp," that is electrons with energies less than ~200 keV arriving later—which is exactly what Arase observes at slightly higher L-shells. It is important to note that inside L=4 background-corrected data is available at all energies measured by the MagEIS instrument. It is also important to note that the intense fluxes at the bottom of the spectrogram are not injected electrons but rather the normal fluxes of medium-energy electrons that are always observed in the slot region and inner radiation belt, as will be discussed in Section 5.

REEVES ET AL. 4 of 16

21699402, 2025, 11, Downloa

ary.wiley.com/doi/10.1029/2025JA034329 by British Antarctic Survey, Wiley Online Library on [03/11/2025]. See the Terms and Conditions (https://onlinelibrary.wiley.com/term

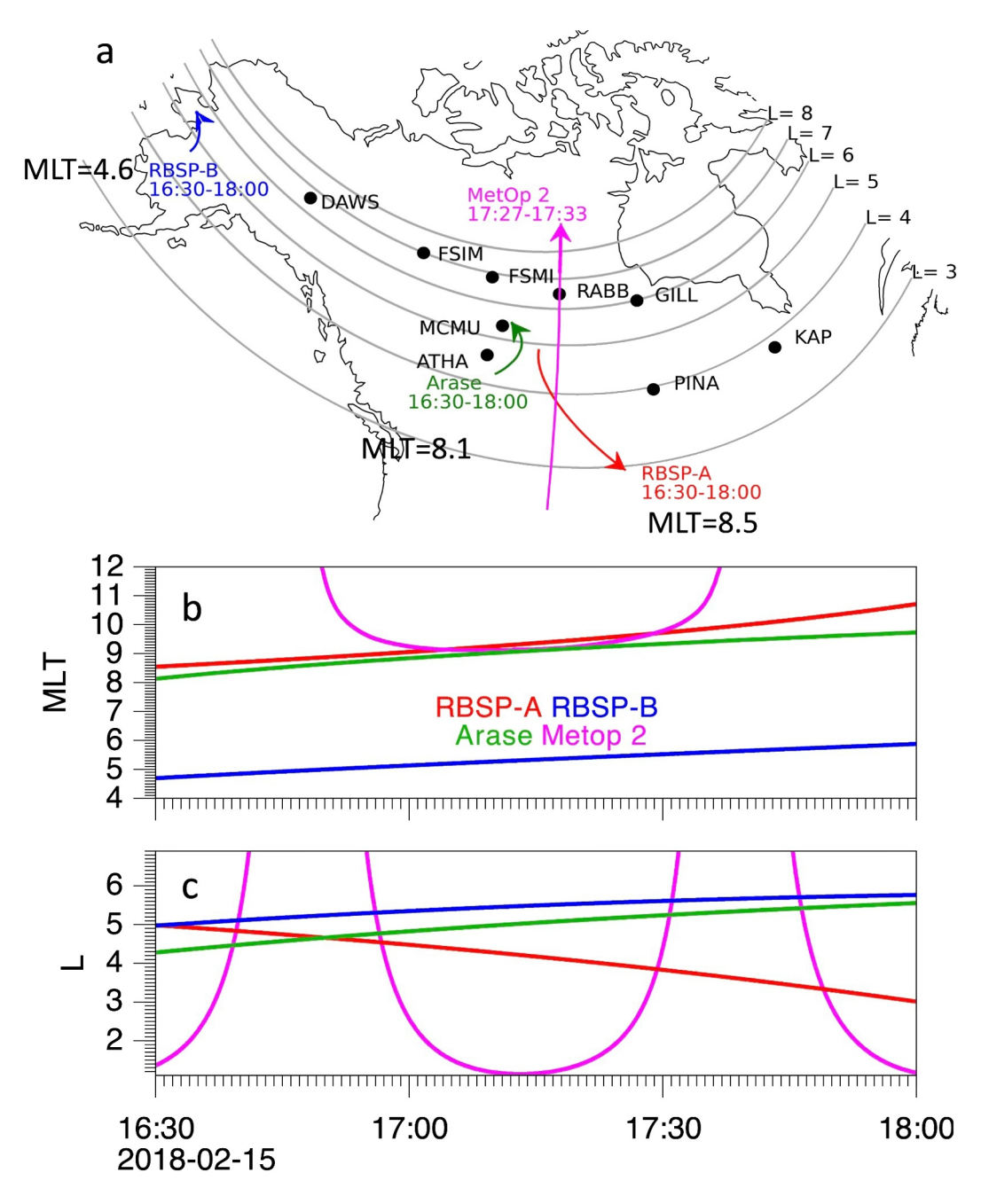


Figure 3. (a) The magnetic footpoints of RBSP-A (red), RBSP-B (blue), MetOp 2 (magenta) and Arase (green) orbits between 1,630 and 18:00 UT. Riometers used in the study are indicated by the black dots. (b) Corresponding magnetic local times and (c) *L*-shells for all spacecraft between 1,630 and 18:00 UT are shown.

We can further investigate the source of the dispersed injection seen by RBSP-A using a simple drift tracing model with no inner boundary to the injection region. To do this we start with an assumed pie-shaped injection region that is 5 hr wide in MLT regardless of L-shell. I.e. 5-hourswide at geosynchronous orbit and 5-hourswide at all L-shells inside geosynchronous orbit down to L=1. We then propagate electrons at different energies from both the eastern and western edges of that wedge. The result, shown in Figure 7, defines the energy- and time-dependent region where injected fluxes could be observed from this hypothetical source. It is clear from this analysis that if electrons had been injected below L < 3.8 they would have been observed by RBSP-A but were not.

REEVES ET AL. 5 of 16

21699402, 2025, 11, Downloaded from https://agupubs.onlinelibrary.wiley.com/doi/10.1029/2025IA034329 by British Antarctic Survey, Wiley Online Library on [03/11/2025]. See the Terms and Condit

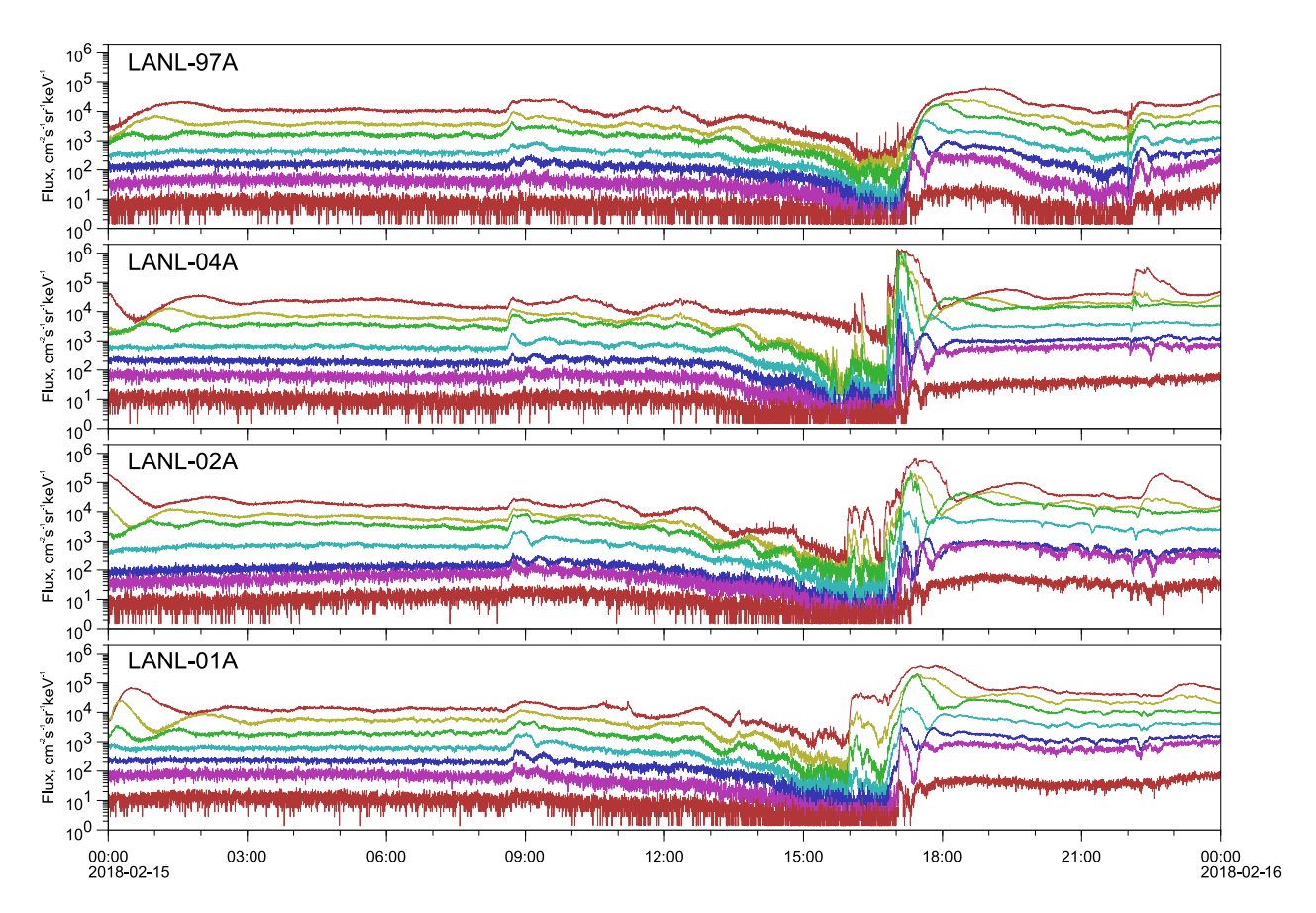


Figure 4. Spin averaged electron flux observed by LANL-GEO satellites. The energies plotted are logarithmically spaced spanning approximately 60-570 keV.

By trial and error, we find that the onset time that best matches the data is 17:07 UT, about 7 min after the dispersionless injection at geosynchronous orbit. This delay is consistent with known, relatively slow, inward propagation of the injection front from the geosynchronous orbit to lower L-shells. A delay of 7 min corresponds to a radial propagation speed of approximately 30–40 km/s, which is roughly consistent with previous studies (Malaspina et al., 2015; Reeves, Friedel, et al., 1996).

Additional justification for the location of the hypothetical injection "wedge" is given in Supporting Information S1 (Section S2) that backward traces the drift of the electrons from the time and location they were observed. Where the drift paths, in UT and MLT, converge indicates the location and time of the dispersionless onset (see e. g. Reeves et al., 1991; Turner et al., 2017).

4. Supporting Observations

4.1. Observations of Electron Precipitation

Ground-based riometers at multiple stations in the Canadian GO-RIO (Spanswick et al., 2025) measure precipitating electrons with energies $\gtrsim 30$ keV. The GO-RIO riometer signals are shown in Figure 8. (The location of the riometer stations and the magnetic foot points of the satellites are shown in Figure 3.) Multiple stations at different L-shells can be used to pinpoint the radial (L-shell) extent of the precipitation. Five stations were located at L > 6, with the other four stations at L = 5.35, L = 4.40, L = 4.06, and L = 3.70. Clear absorption signatures were observed down to L = 4.4 but not at lower L-shells.

Figure 8b zooms in on precipitation signatures from 5 stations in the time range 17:00–20:00 UT. Furthermore, we convert the riometer voltage into absorption in dB by subtracting riometer voltages from station-specific geomagnetically quiet days. By computing the time lag differences between pairs of stations in the East-West chain of riometers using cross-correlation analysis (Figure 8c), we observe that the precipitation events occur

REEVES ET AL. 6 of 16

21699402, 2025, 11, Downl

from https://agupubs.onlinelibrary.wiley.com/doi/10.1029/2025JA034329 by British Antarctic Survey, Wiley Online Library on [03/11/2025]. See the Terms and Condition

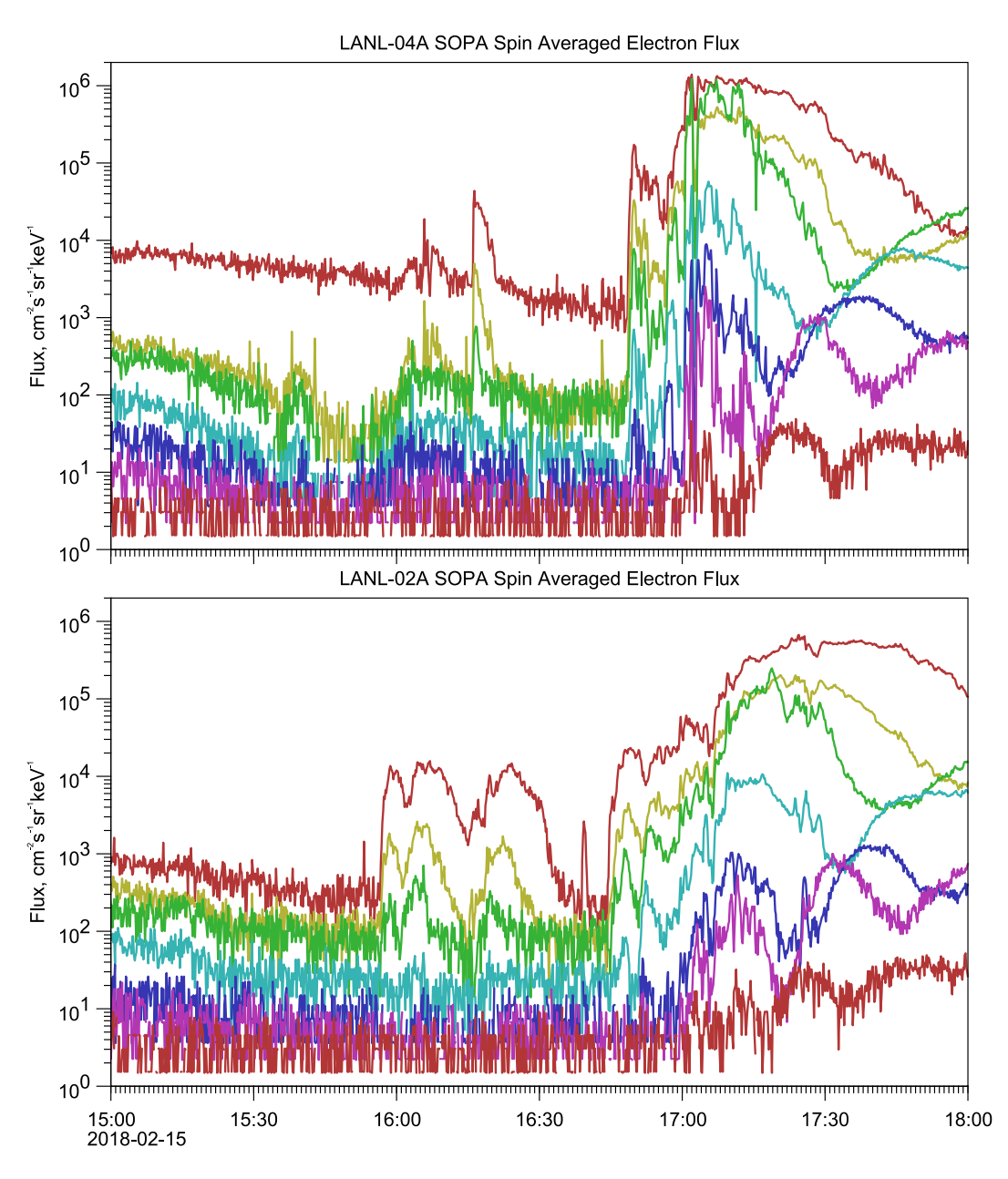


Figure 5. An expanded set of times from Figure 4 from 15:00 to 18:00 UT for LANL-04A (top) and LANL-02A (bottom). The energies plotted are logarithmically spaced spanning approximately 60–570 keV.

within ± 4 min across these stations. These stations span a sector equivalent to approximately 4 hr in MLT. This allows more precise temporal assessment. For comparison, the theoretical time for a 100 keV electron to drift around the Earth is 2 hr at L=4 and 1.5 hr at L=5. At 300 keV, the drift periods are 45 min at L=4 and 36 min at L=5. This means that the electron injection is covering a wide range of MLT. From this analysis, it appears that the observed synchronization with such short time lags suggests that the spatial extent of the precipitation patch is at least 4 hr in MLT and the energy of the precipitating particles extends to at least 300 keV.

Observations from Medium Energy Proton and Electron Detector instrument on the MetOp 2/POES satellite confirm the precipitation of electrons over the Canadian sector for this time period. Figure 9 shows trapped (black) and precipitating (red) electron fluxes at several energies. The nearly equal flux levels for energies up to several hundred keV are indicative of enhanced electron precipitation, which was likely caused by wave-induced pitch angle scattering as discussed in the next section.

REEVES ET AL. 7 of 16

21699402, 2025, 11, Downloaded from https://agupubs.onlinelibrary.wiley.com/doi/10.1029/2025JA034329 by British Antarctic Survey, Wiley Online Library on [03/11/2025]. See the Terms

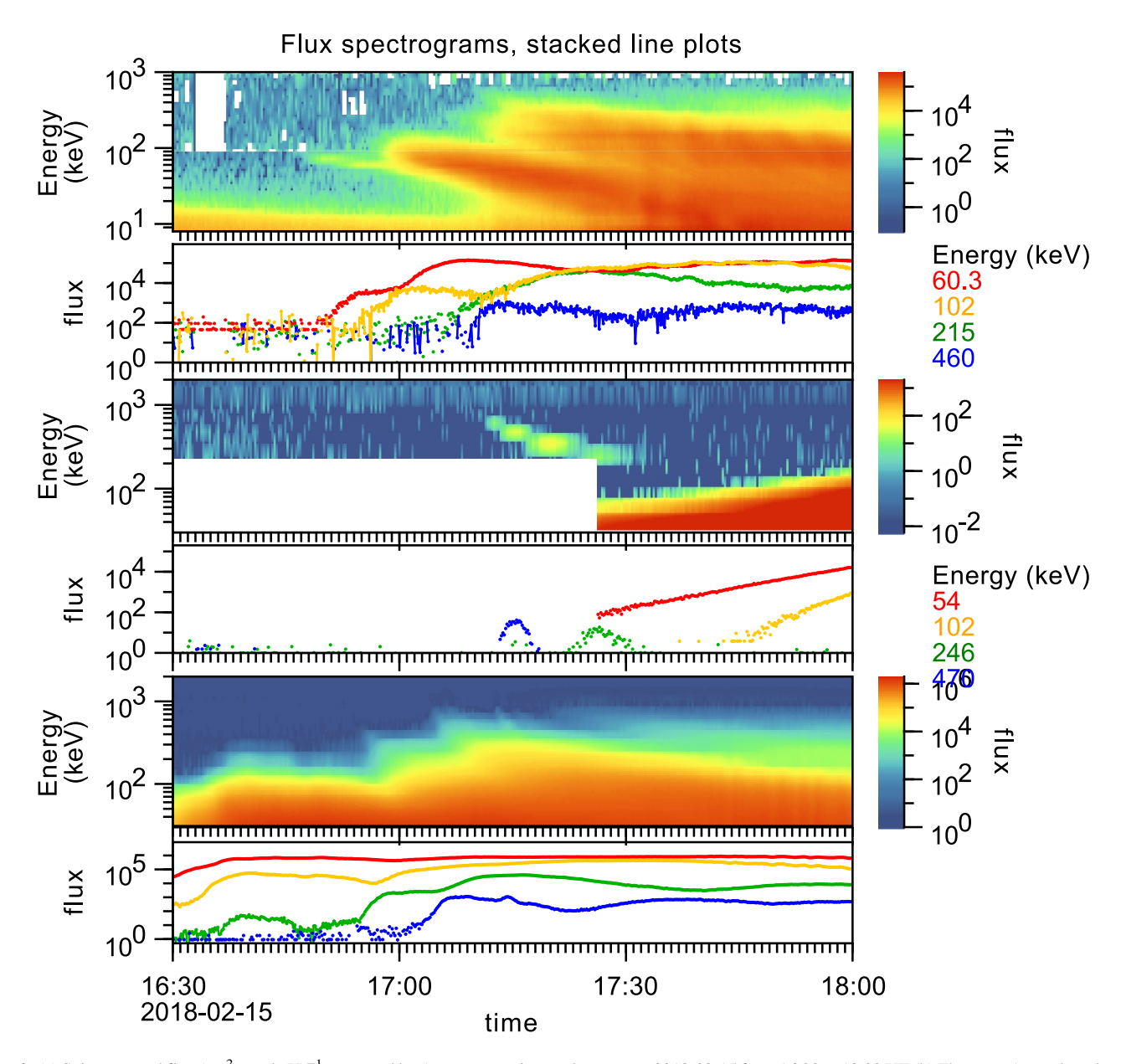


Figure 6. (a) Spin averaged flux (cm²-s-sr-keV)⁻¹ measured by Arase versus time and energy on 2018-02-15 from 16:30 to 18:00 UT (b) The same Arase data shown as stacked line plots at selected energy channels. Energy versus time and stacked line plots for (c and d) RBSP-A and (e and f) RBSP-B. The Energy-Time plots show the full spectral information, while the line plots more clearly illustrate the time evolution of fluxes at particular energies.

4.2. Electromagnetic Waves Produced by the Injection

RBSP-A was in the plasmasphere from 16:00 to 18:00 as indicated by cold plasma densities greater than 250 #/cc (Figure 10a) when it observed whistler-mode hiss waves (Figures 10b and 10c). On the contrary, RBSP-B was located in the plasmapause transition region (Ripoll et al., 2022) with density close to 100 #/cc from 16:00 and 16:30 UT and in the plasma trough between 16:30 and 18:00 UT where clear whistler-mode chorus wave activity was observed (not shown).

As seen in Figures 10b and 10c, hiss waves observed by RBSP-A are split into two populations, one at lower frequency and the other at higher frequency. The two-band hiss structure observed during this interval has morphology consistent with recent studies of banded hiss (e.g., Ni et al., 2023). The lower-frequency limit of the lower-band hiss is plotted in Figures 10b and 10c with a black dashed line. The spectrograms show a minimum in power spectral density between the upper and lower bands, which we call the "split frequency" (plotted with a

REEVES ET AL. 8 of 16

21699402, 2025, 11, Downloaded from https://agupubs.onlinelibrary.wiley.com/doi/10.1029/2025JA034329 by British Antarctic Survey, Wiley Online Library on [03/11/2025]. See the Terms and Conditions

(https://onlinelibrary.wiley.com/terms-and-conditions) on Wiley Online Library for rules of use; OA articles are governed by the applicable Creative Commons Licens

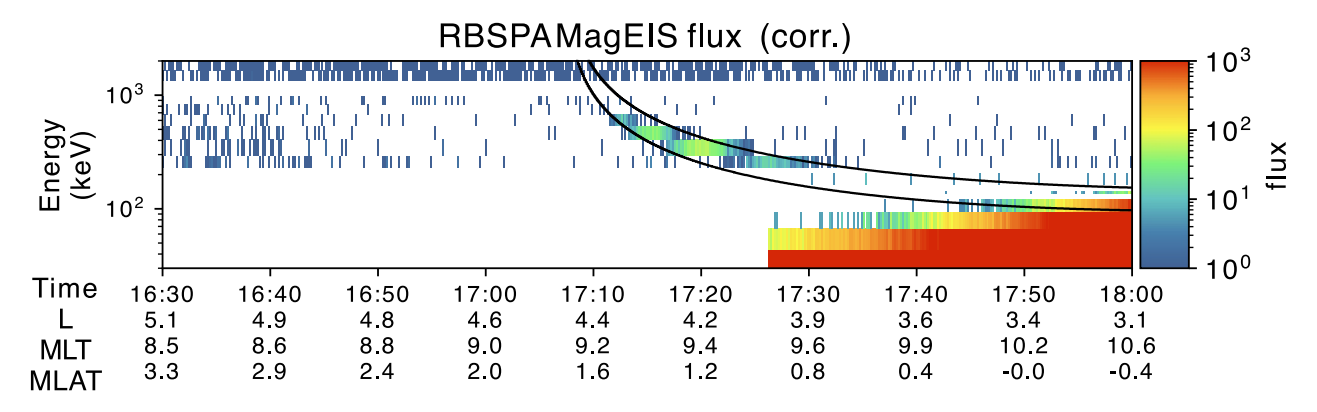


Figure 7. Spin averaged flux (cm²-s-sr-keV)⁻¹ measured by RBSP-A as in Figure 6 (With a change of color bar.). The two black curves show the expected arrival times of electrons from the Eastern (earlier times) and Western (later times) of a hypothetical injection "wedge," 5 hr wide in magnetic local time in the midnight sector starting at 17:07 UT.

magenta dashed line). The split frequency was determined manually at each time step and is essentially the upper frequency limit of the lower-frequency population of waves. Lower band hiss waves between 30 and 300 Hz occur from 16:30 to 18:00 (Figures 10b and 10c). They intensified from 16:45 to 17:45 UT between L = 4.8 and L = 3.5.

The information in Figure 10 can be used to determine if the locally observed population of injected electrons (Figure 7) might be the source of the locally observed hiss waves. Figure 10d shows the resonance energy of

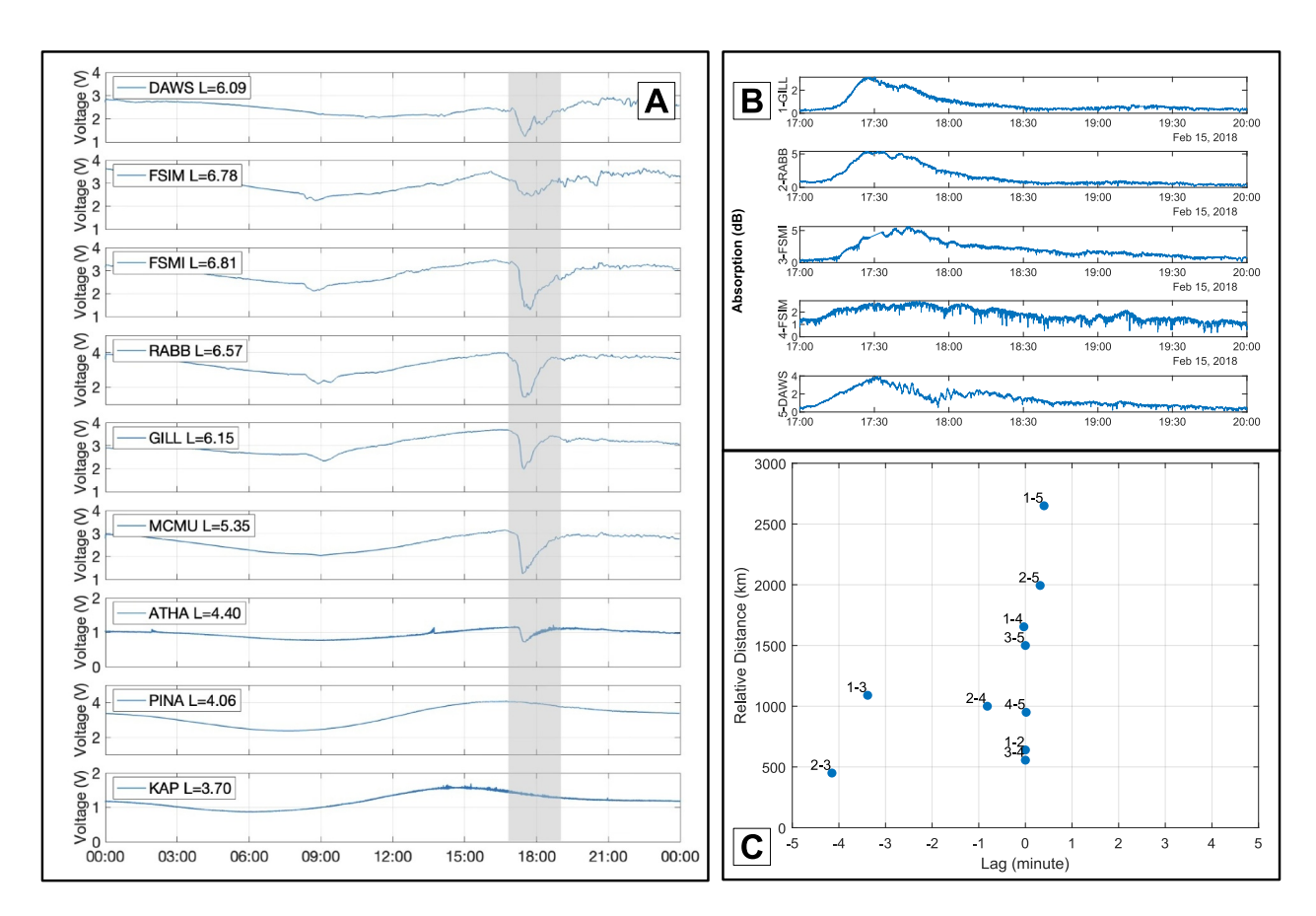


Figure 8. (a) Absorption data from riometers in the Geospace Observatory Riometer Network array. Figure 3 shows a map of the station locations and their L-shells are labeled in each panel. (b) Absorption in dB by the (from top to bottom) GILL, RABB, FSMI, FSIM, and DAWS riometers. (c) Time lag, in minutes, of the precipitation observed by the riometers sorted by their respective distances between pairs of them.

REEVES ET AL. 9 of 16

21699402, 2025, 11, Downloa

ded from https://agupubs.onlinelibrary.wiley.com/doi/10.1029/2025JA034329 by British Antarctic Survey, Wiley Online Library on [03/11/2025]. See

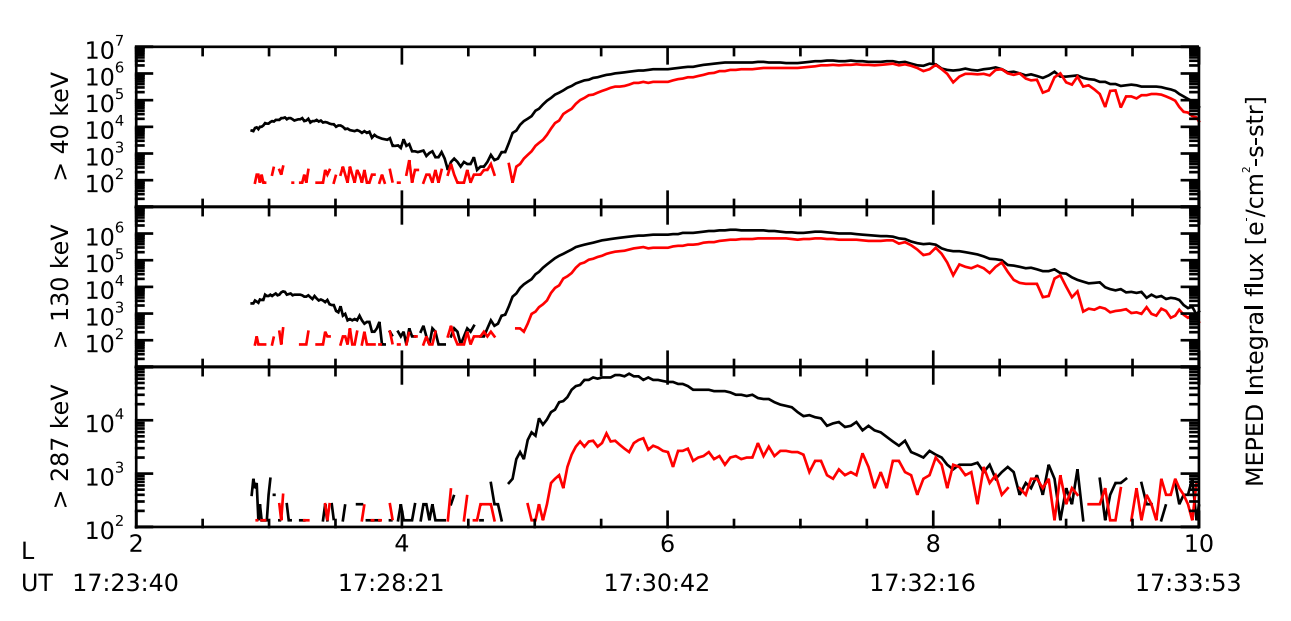


Figure 9. Medium Energy Proton and Electron Detector Integral Flux (e/cm2.s.str) of (red) precipitating and (black) trapped electrons observed by MetOp 2.

electrons that can efficiently interact with the low frequency hiss waves observed by RBSP-A between the lower frequency limit (black) and the split frequency (magenta). The resonance energy is given by

$$E_{\rm res} = m_e c^2 (\gamma_{\rm res} - 1) \text{ with } \gamma_{\rm res} = \sqrt{1 + p_{\rm res}^2}$$
 (1)

The resonant electron momentum is obtained through Equation 8 of Mourenas and Ripoll (2012) for the n = -1 cyclotron resonance

$$p_{\text{res}} = (\omega_{ce}/\omega_{pe}) * (\omega_{ce}/\omega_{\text{res}} \cos(\theta))^{1/2}$$
(2)

Here, m_e is the mass of an electron, c is the speed of light, ω_{ce} is the local electron cyclotron frequency, ω_{pe} is the local electron plasma frequency, and ω_{res} is the resonant wave frequency (i.e., the observed wave frequency). The observed wave normal angle, θ , is close to zero during this interval (See Kletzing et al., 2023). By evaluating ω_{res} at both the split frequency (magenta dashed line Figures 10b and 10c) and the lower frequency bound (black dashed line in Figures 10b and 10c), we are able to plot the range of resonant energies as a function of time as RBSP-A enters deeper into the plasmasphere. In this way, we seek to determine whether the local generation of hiss waves can be attributed to a resonant process with the injected electrons.

The first notable result is the absence of lower band hiss waves when the resonant energy is around 10 keV (from 16:00 to 16:30) and RBSP-A is located between L = 5.5 and L = 5. The appearance of lower band hiss waves coincides with a shift in resonant energies above 20-30 keV. Note that the cold plasma electron density observed by RBSP-A remains consistently high from 16:00 to 17:30 at about 250 #/cc.

The arrival times of injected electrons are plotted in panel d as red dots (see Figure 7 for the complete data). The dotted box delimits ~17:05–17:30 UT for reference. Examining the energy of the injected electrons, we see that the minimum frequency for the hiss waves also decreases as lower-energy electrons arrive (panels b and c). The peak hiss wave intensity occurs at about 17:20 UT when the resonant energy is in the 100–200 keV range, which is the energy at which the highest injected fluxes are observed. The hiss intensity then falls as RBSP-A enters deeper into the plasmasphere The diminishing of hiss amplitude coincides with higher resonant energies, ~500 keV, where the flux of injected electrons is much lower.

These results suggest that substorm-injected electrons of energy up to several hundred keV are the source of local low frequency hiss waves. Prior studies have shown that >100 keV electrons can drive lower band hiss waves in

REEVES ET AL. 10 of 16

21699402, 2025, 11, Downloaded from https://agupubs.onlinelibrary.wiley.com/doi/10.1029/2025/A034329 by British Antarctic Survey, Wiley Online Library on [03/11/2025]. See the Terms and Conditional Conditions of the Conditional Condition of the Condition of the Conditional Condition of the Cond

and-conditions) on Wiley Online Library for rules of use; OA

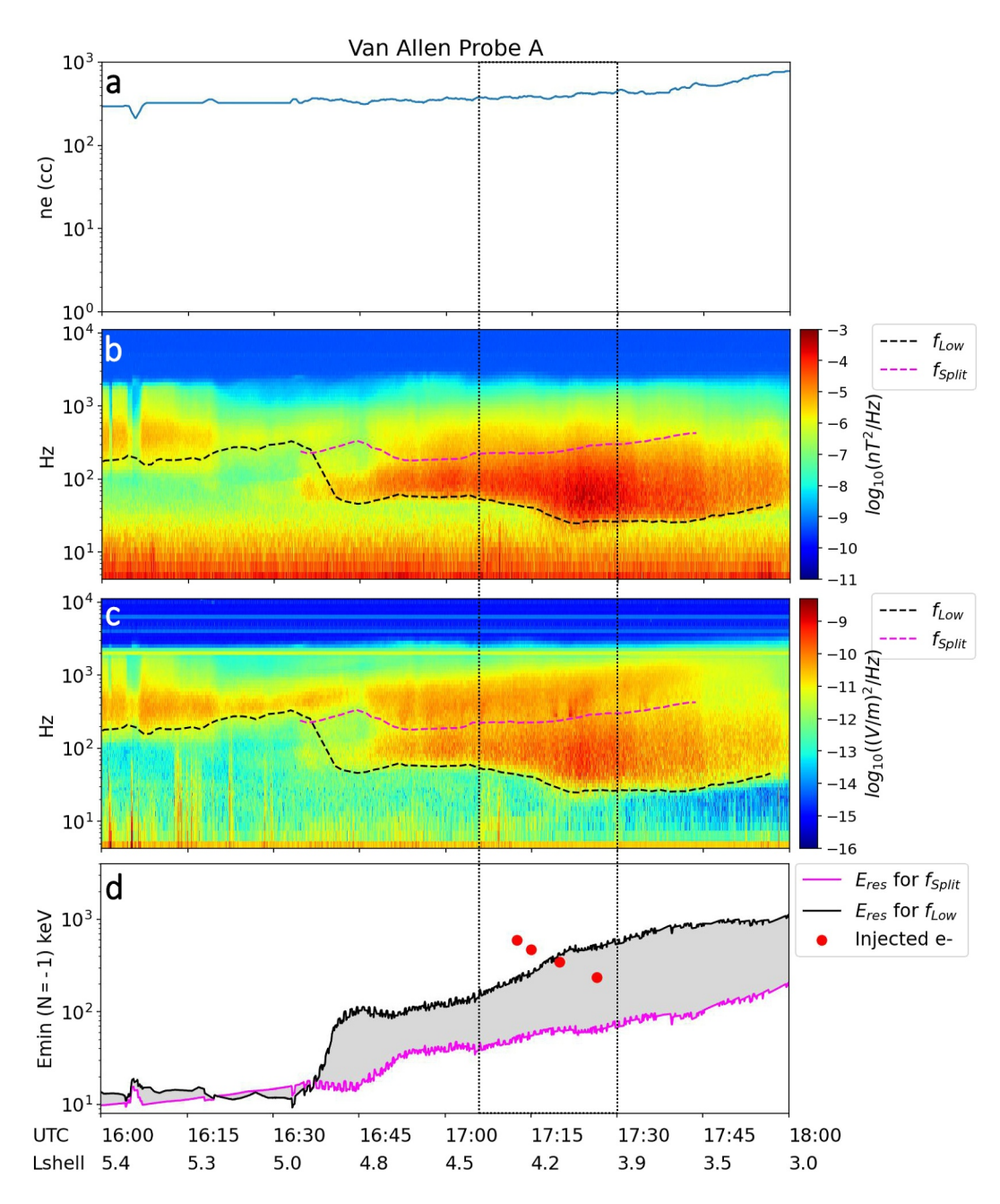


Figure 10. (a) Cold plasma density, (b) electric field and (c) magnetic field power spectral density measured by RBSP-A in the plasmasphere on 2018-02-15 from 16:00 to 18:00 UT. In (b) and (c), the black dashed line indicates the lower frequency bound of the hiss waves. The magenta dashed line indicates a frequency that splits lower and upper hiss frequencies. (d) The wave-resonant energies, in keV, of hiss waves between the lower bound hiss frequency and the hiss split frequency (computed for cyclotron N = -1 resonance). The energy of the observed injected electrons (cf. Figure 7) is indicated by red dots.

the plasmasphere (e.g., Li et al., 2013), this is the first time to the authors' knowledge that a coincident observation of a localized electron injection and corresponding hiss wave power has been shown.

5. Electron Transport in the Slot Region

In some geomagnetic storms, energetic particles have been seen to penetrate through the slot region and into the inner radiation belt and have been referred to as "slot-filling events" or "slot-filling injections" (e.g.., Baker et al., 2004; Reeves et al., 2016; Turner et al., 2015). Several important observations help to establish the

REEVES ET AL. 11 of 16

21699402, 2025, 11, Downloaded from https://agupubs.onlinelibrary.wiley.com/doi/10.1029/2025IA034329 by British Antarctic Survey, Wiley Online Library on [03/11/2025]. See

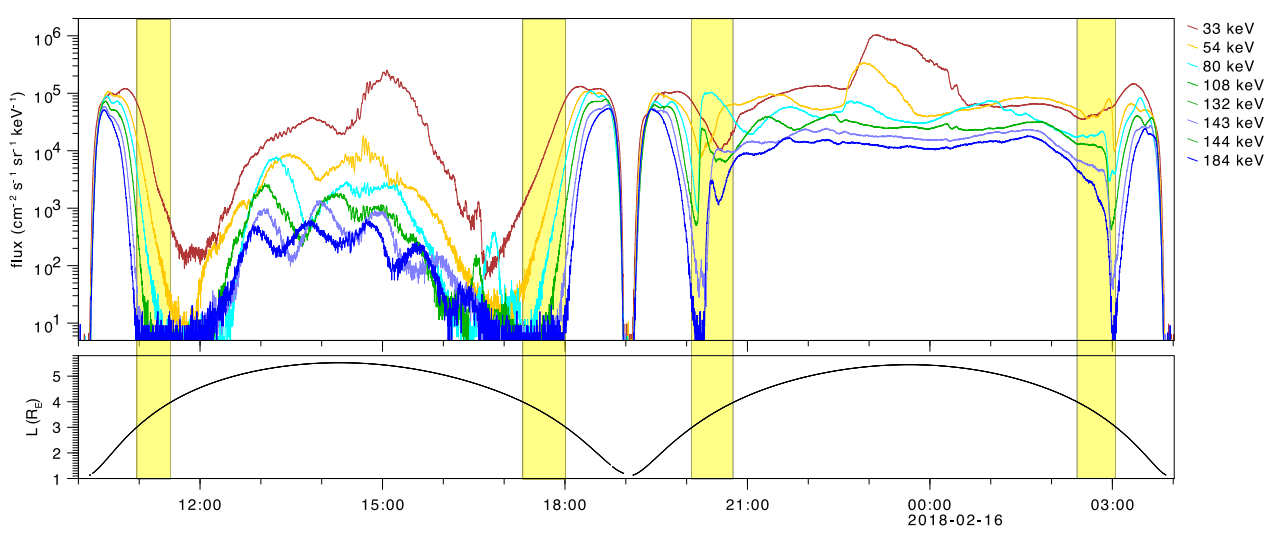


Figure 11. MagEIS data from RBSP-A for two full orbits showing electrons filling the nominal slot region. In the top plot MagEIS data is shown for energies from 33 to 184 keV and the bottom plot shows the L-shell. Yellow highlighted areas show when RBSP-A is between L = 3 and L = 4.

differences between slot-filling events and the more commonly observed substorm injections. In slot-filling events, only electrons, not ions, are transported to low L-shells. Additionally, in slot-filling events, lower-energy electrons penetrate lower L-shells than the higher-energy electrons (Reeves et al., 2016; Turner et al., 2015). In contrast, for substorms, electrons and ions across the full range of energies are injected simultaneously and in the same region of space (commonly referred to as the "dispersionless" injection region). Therefore, as Turner et al. (2015) conclude "it is evident that these low L injections may result from a very different mechanism than injections at higher L shells."

Nevertheless, previous studies have not ruled out substorm-associated processes as responsible for both dispersionless injections and slot-penetrating events. For example, Turner et al. (2015) consider the electric field associated with dipolarizing magnetic fields (Nosé et al., 2010; Ohtani et al., 2007) and/or low-entropy plasma bubbles (e.g., Sorathia et al., 2021; Wolf et al., 2006, 2009) but conclude those are unlikely causes for the events considered. Sergeev et al. (1998) suggested that fast magnetosonic waves could be launched as the substorm injection comes to a stop in the inner magnetosphere and hence further transport electrons across dipole-like field lines. Turner et al. (2015) also proposed that slot-filling events could "result from localized drift resonance with fast magnetosonic cavity mode waves in the Pi2 frequency range that are generated by dipolarization fronts braking at higher *L* shells." In contrast, Lejosne et al. (2018) propose that slot-filling events result from the electric field structures inside Sub-Auroral Polarization Streams (SAPS) (Anderson et al., 2001; Foster et al., 2007, 2014; Goldstein et al., 2003). SAPS are known to be long-lasting, occur equator-ward of the auroral zone, and do not overlap spatially or temporally with dispersionless substorm injections. Understanding the spatial and temporal co-occurrence (or absence thereof) provides important information for further exploration of these events.

The event of 15 February 2018 and subsequent days provides a unique opportunity to examine the relationship of slot-filling events to substorm injections. We have already established that the substorm injection on February. 15 did not inject electrons below L=3.8-3.9 and therefore did not fill the slot at that time. Figure 11, however, shows RBSP-A data for two complete orbits (\sim 18 hr) extending into Feb. 16, which does show electrons with energies >100 keV completely filling the slot region down to at least L<3.

To understand the events at low L-shells it is important to first look at the quiet-time structure of the medium energy inner radiation belt electrons (e.g., Reeves et al., 2016; Ripoll et al., 2016, 2019). At the beginning of these two orbits (\sim 10:00 UT on 15 February), RBSP is moving outward from the perigee seeing first high fluxes, then a deep minimum (slot), followed by increasing fluxes out to apogee at $L \approx 5.8$. While these are not, strictly, radiation belt electrons, the medium energy (10–100 s keV) flux profiles still show the inner zone–slot–outer zone structure of their more energetic counterparts. In the "inner zone," lower-energy electrons extend to higher L-shells than higher energy electrons appearing as a "wedge" in Energy-L-shell format (see Reeves et al., 2016). (Here, unlike Figure 6, we plot uncorrected RBSP-A/MagEIS fluxes so that the flux profiles are continuous with

REEVES ET AL. 12 of 16



Journal of Geophysical Research: Space Physics

10.1029/2025JA034329

no gaps. While this results in a higher "noise" floor—see, for instance the 33 keV minimum fluxes—the background contamination for this period is orders of magnitude lower than the fluxes of interest.)

From $\sim 15:30$ to $\sim 16:00$ UT we see the substorm activity that was also observed at geosynchronous orbit (cf. Figures 4 and 5). Shortly after 17:00 we see the "wisp" of drifting, dispersed electrons from Figures 6 and 7. We see here, more clearly, that substorm-injected electrons with energies < 54 keV were not observed below L = 3.8-3.9 and did not fill the slot. Note, also, that in slot-penetrating events lower-energy electrons are always transported to lower L-shells than higher-energy electrons (e.g., Reeves et al., 2016; Turner et al., 2015).

Following the injection, RBSP-A again moves into and back out of the perigee. On the inbound leg, the electron flux gradients remain unchanged except for magnetic latitude-related orbital effects. However, on the subsequent outbound pass, there is a considerable change in fluxes in the slot region as electrons are transported through the slot, up against the steep radial gradients of the inner zone. By the subsequent pass (02:00-04:00 UT on 16 February), the 33 keV electrons have completely filled the slot and the peak of 54 keV electron fluxes in the slot are comparable to or greater than the peak in the inner zone. The slot remains full or elevated for days until whistler-mode hiss scatters those electrons into the atmosphere over the next $\sim 5-10 \text{ days}$ (e.g., Shprits et al., 2005; Ripoll., 2016).

Thus, the different signatures of the substorm injection and the slot-filling events are seen to be spatially and temporally separated but do they have distinctly different causes? Part of the answer lies in close examination of Figures 1, 4 and 5. At geosynchronous orbit, all of the substorm-related injection activity is over before 17:30 UT. The only significant signatures between \sim 17:15 UT and \sim 22:30 UT are the "drift echos", which are observed when the electrons of a given energy have circled the Earth to be observed again at the same location. Drift echos are only clearly observed when the post-injection magnetosphere is quiet. The lack of substorm activity in this period is consistent with the AE index (Figure 1), which dropped below, and stayed below 400 nT starting at \sim 18:10 UT on 15 February.

We conclude that the substorm injection and slot-filling events (at least in this case) result from spatially and temporally distinct processes. However, it is very possible, and perhaps likely that substorm injections are a necessary and required precursor—producing an enhanced population of energetic electrons just outside the slot region that are then available for subsequent further transport into and through the slot region.

6. Summary and Conclusions

We examined several features of an injection event observed by a large number of fortuitously located satellites and ground stations. The event was identified through coordinated analysis over several workshops at the International Space Science Institute (ISSI) in Bern dedicated to joint analysis of multi-platform observations. The events in question were embedded within a CIR which initiated a moderate geomagnetic storm. The energetic particle injection at the beginning of that storm and subsequent observations at low L-shells show several interesting features that the authors believe have not been previously reported.

A series of storm-time substorm injections were observed at geosynchronous orbit both as local, dispersionless injections and as energy dispersed (drifting) injected electrons. The main dispersionless injection at geosynchronous orbit showed similar temporal features observed simultaneously at 21 and 02 MLT and therefore spanned \sim 5 hr in MLT around magnetic midnight.

As seen in previous studies, the injected population was also observed well inside the geosynchronous orbit. The radial and azimuthal shape of the "injection boundary" was first proposed by McIlwain (1974) and Mauk and Mcilwain (1974). The injections propagate Earthward with velocities of 10s km/s, which is consistent with the velocities estimated for this event (cf. Section 2.2). It has generally been assumed that they slow and eventually stop as they encounter strong dipole-like field lines. They should, therefore have a minimum radial boundary, which probably varies from event to event. In this event, we were able to, for the first time, precisely specify the location of that inner radial injection boundary. For this event, it was at L = 3.8-3.9, well inside the plasmasphere.

All satellites and ground stations outside the midnight sector observed the injection as drifting energy-dispersed signatures. At the time of the injection, RBSP-A was on the inbound leg of its orbit and Arase was outbound in the same local time sector ~ 9 MLT (Figure 2). The main injection arrived at both satellites around 17:10 UT. As

REEVES ET AL. 13 of 16

21699402, 2025, 11, Downloaded from https://agupub

m/doi/10.1029/2025JA034329 by British

Wiley Online Library on [03/11/2025]. See the Terms

Acknowledgments

This research was supported by the International Space Science Institute

(ISSI) in Bern through ISSI International

Team project #477 (Radiation Belt Physics From Top To Bottom: Combining

Multipoint Satellite Observations And

Data Assimilative Models To Determine The Interplay Between Sources And

Losses) with J.-F Ripoll and G.D. Reeves,

co-leaders. This work was also supported

Research, Nagoya University. The authors

thank the EFW and EMFISIS teams of the

Y. Ogawa for operations and data from the

Tromsø all sky cameras, Dr. M. Henderson

for processing the LANL-GEO Data, and E. Spanswick for the operation of and data

from the GO-RIO stations. The work of

J-FR and GC was performed under the auspices of an agreement between CEA/

Atomique, Direction des Applications Militaires) and NNSA/DP (National Nuclear Security Administration, Defense

Program) on cooperation on fundamental science. J-FR thanks the Direction

Générale de l'Armement (DGA) and the Agence pour l'Innovation de Défense (AID) for funding the ASTRID project

"PACTE- ESPACE." CMC acknowledges the support of the Natural Sciences and

Engineering Research Council of Canada (NSERC), funding reference number

RGPIN-2020-05219. VP thanks the project

21GRD02 BIOSPHERE that has received

funding from the European Partnership on

Metrology, co-financed by the European Union's Horizon Europe Research and

Innovation Programme. Processing and

Instrument Suite and Integrated Science

(EMFISIS), and the Electric Fields and

Waves (EFW) investigations were funded

under NASA's Prime contract no. NAS5-

01072

analysis of the Van Allen Probes data was supported by the Energetic Particle, Composition, and Thermal Plasma (RBSP-ECT), the Electric and Magnetic Field

DAM (Commissariat à l'Energie

by the joint research program of the Institute for Space-Earth Environmental

Van Allen Probes mission for their support. We would also like to thank Prof.

Journal of Geophysical Research: Space Physics

Arase moved outward from $L \sim 4.5$ to $L \sim 5.2$ it continued to measure the injection down to energies of $\lesssim 30$ keV. In contrast, RBSP-A, moving inbound, saw only a weak "wisp" of injected electrons at high energies, from ~ 200 to ~ 600 keV, which ended at $\sim 17:30$ UT when RBSP-A was at L = 3.8-3.9. The combination of Arase and RBSP-A observations of the same injection near the same point in space is key to identifying L = 3.8-3.9 as the inner edge of the injection region for this event. If injected electrons had been present below L < 3.8, RBSP-A would have observed the continuation of the "wisp," that is, electrons with energies less than ~ 200 keV arriving later—but it did not.

More evidence supporting this conclusion comes from ground observations and satellite observations of whistler mode hiss. Ground riometer stations in excellent magnetic conjunction with Arase and RBSP-A showed signatures of strong energetic electron precipitation from L > 6 down to at least L = 4.4. Observations from the LEO satellite MetOP 2 confirm the presence of electron precipitation in that region at the same time.

Throughout most of its inbound orbit, from 16:00 to 18:00 UT, RBSP-A observed whistler mode hiss inside the plasmasphere. The hiss was clearly divided into an upper and lower frequency band. We present an analysis of the wave-particle resonance condition for determining the minimum-frequency lower band hiss and the frequency that splits the lower and upper band emissions. The resonant energies correspond very well with the energies of the injected electrons observed at the same location, suggesting that the substorm-injected electrons are the source of the local low frequency hiss waves. Prior studies have shown that 100 s keV electrons can drive lower band hiss waves (e.g., Li et al., 2013), this is the first time to the authors' knowledge that a coincident observation of a localized electron injection and corresponding hiss wave power is shown.

Finally, to further investigate the relationship between substorm injections and "slot-filling" events, we examined the energetic electron dynamics following the injection (i.e., 17:30 UT on Feb. 15 to 04:00 UT on 16 February). We compared two orbits (\sim 18 hr) of data from RBSP-A as it passed through the inner zone, slot region, and outer zone, highlighting times when the satellite passed through L=3-4. Comparing the inbound pass after the 17 UT injection with the subsequent outbound and inbound passes shows considerable changes in the electron fluxes observed in the slot region. Electrons with energies up to at least 130 keV completely penetrated the slot region merging into the pre-existing, relatively stable populations trapped at low L-shell. Notably, no new substorm injection activity was observed between \sim 17:15 UT and \sim 22:30 UT so we rule out the possibility that the slot-filling was caused by additional substorm injections. These observations show that the earlier substorm injection and the later slot-filling event were both temporally and spatially distinct processes. It is still likely, however, that substorm injections are a necessary and required precursor - producing an enhanced population of energetic electrons outside the slot region that are available for subsequent further transport into and through the slot region.

Further observational and model-based studies of this event, both the injection and subsequent slot-filling are underway.

Conflict of Interest

The authors declare no conflicts of interest relevant to this study.

Data Availability Statement

MagEIS data is available at https://cdaweb.gsfc.nasa.gov/pub/data/rbsp/rbspa/12/ect/. EMFISIS data is available at https://cdaweb.gsfc.nasa.gov/pub/data/rbsp/rbspa/12/emfisis/wfr/. Arase/ERG data is available at https://ergsc.isee.nagoya-u.ac.jp/data_info/erg.shtml.en. GO-RIO riometer data is available at https://www.ucalgary.ca/aurora/projects/rio. OMNI data are available at https://omniweb.gsfc.nasa.gov/. Tromsø all sky camera data is available at https://www.isee.nagoya-u.ac.jp/doi/10.34515/DATA_GND-0059-0006-0201_v01.html. LANL-GEO data and other data collected from the preceding repositories is available at https://doi.org/10.5281/zenodo. 15285033 (Reeves, G. D., 2025).

References

Anderson, P. C., Carpenter, D. L., Tsuruda, K., Mukai, T., & Rich, F. J. (2001). Multisatellite observations of rapid subauroral ion drifts (SAID). *Journal of Geophysical Research*, 106(A12), 29585–29599. https://doi.org/10.1029/2001ja000128

Baker, D. N., Kanekal, S. G., Li, X., Monk, S. P., Goldstein, J., & Burch, J. L. (2004). An extreme distortion of the Van Allen belt arising from the Halloween solar storm in 2003. *Nature Letters*, 432(7019), 878–881. https://doi.org/10.1038/nature03116

REEVES ET AL. 14 of 16



Journal of Geophysical Research: Space Physics

- 10.1029/2025JA034329
- Belian, R. D., Cayton, T. E., Christensen, R. A., Ingraham, J. C., Meier, M. M., Reeves, G. D., & Lazarus, A. J. (1996). Relativistic electrons in the outer-zone: An 11 year cycle; their relation to the solar wind. In G. D. Reeves (Ed.), Workshop on the Earth's trapped particle environment (pp. 13–18). AIP Press.
- Blake, J. B., Carranza, P. A., Claudepierre, S. G., Clemmons, J. H., Crain, W. R., Dotan, Y., et al. (2013). The magnetic electron ion spectrometer (MagEIS) instruments aboard the radiation belt storm probes (RBSP). Spacecraft, Space Science Reviews, 179(1–4), 383–421. https://doi.org/10.1007/S11214-013-9991-8
- Borovsky, J. E., & Denton, M. H. (2006). Differences between CME-driven storms and CIR-driven storms. *Journal of Geophysical Research*, 111(A7). https://doi.org/10.1029/2005ja011447
- Claudepierre, S. G., O'Brien, T. P., Blake, J. B., Fennell, J. F., Roeder, J. L., Clemmons, J. H., et al. (2015). A background correction algorithm for Van Allen probes MagEIS electron flux measurements. *Journal of Geophysical Research: Space Physics*, 120(7), 5703–5727. https://doi.org/ 10.1002/2015JA021171
- Foster, J. C., Erickson, P. J., Coster, A. J., Thaller, S., Tao, J., Wygant, J. R., & Bonnell, J. W. (2014). Storm time observations of plasmasphere erosion flux in the magnetosphere and ionosphere. *Geophysical Research Letters*, 41(3), 762–768. https://doi.org/10.1002/2013gl059124
- Foster, J. C., Rideout, W., Sandel, B., Forrester, W. T., & Rich, F. J. (2007). On the relationship of SAPS to storm-enhanced density. *Journal of Atmospheric and Solar-Terrestrial Physics*, 69(3), 303–313. https://doi.org/10.1016/j.jastp.2006.07.021
- Friedel, R. H. W., Korth, A., & Kremser, G. (1996). Substorm onsets observed by CRRES: Determination of energetic particle source regions. *Journal of Geophysical Research*, 101(A6), 13137–13154. https://doi.org/10.1029/96ja00399
- Goldstein, J., Sandel, B. R., Hairston, M. R., & Reiff, P. H. (2003). Control of plasmaspheric dynamics by both convection and sub-auroral polarization stream. Geophysical Research Letters, 30(24). https://doi.org/10.1029/2003gl018390
- Gosling, J. T., Borrini, G., Asbridge, J. R., Bame, S. J., Feldman, W. C., & Hansen, R. T. (2012). Coronal streamers in the solar wind at 1 AU. Journal of Geophysical Research, 86(A7), 5438–5448. https://doi.org/10.1029/JA086iA07p05438
- He, Z., Dai, L., Wang, C., Chen, T., Duan, S., & Roth, I. (2023). Characteristics of isolated and storm-time ion injections. *Journal of Geophysical Research: Space Physics*, 128(3), e2022JA030745. https://doi.org/10.1029/2022ja030745
- Henderson, M. G., Skoug, R., Donovan, E., Thomsen, M. F., Reeves, G. D., Denton, M. H., et al. (2006). Substorms during the 10–11 August 2000 sawtooth event. *Journal of Geophysical Research*, 111(A6). https://doi.org/10.1029/2005ja011366
- Kasahara, S., Yokota, S., Mitani, T., Asamura, K., Hirahara, M., Shibano, Y., & Takashima, T. (2018). Medium-energy particle experiments— Electron analyzer (MEP-e) for the exploration of energization and radiation in geospace (ERG) mission. Earth Planets and Space, 70(1), 69. https://doi.org/10.1186/s40623-018-0847-z
- Kletzing, C. A., Bortnik, J., Hospodarsky, G., Kurth, W. S., Santolik, O., Smitth, C. W., et al. (2023). The electric and magnetic fields instrument suite and integrated science (EMFISIS): Science, data, and usage best practices. *Space Science Reviews*, 219(4), 28. https://doi.org/10.1007/s11214-023-00973-z
- Lejosne, S., Kunduri, B. S. R., Mozer, F. S., & Turner, D. L. (2018). Energetic electron injections deep into the inner magnetosphere: A result of the subauroral polarization stream (SAPS) potential drop. *Geophysical Research Letters*, 45(9), 3811–3819. https://doi.org/10.1009/2018/GI-077060
- Li, W., Thorne, R. M., Bortnik, J., Reeves, G. D., Kletzing, C. A., Kurth, W. S., et al. (2013). An unusual enhancement of low-frequency plasmaspheric hiss in the outer plasmasphere associated with substorm-injected electrons. *Geophysical Research Letters*, 40(15), 3798–3803. https://doi.org/10.1002/grl.50787
- Malaspina, D. M., Wygant, J. R., Ergun, R. E., Reeves, G. D., Skoug, R. M., & Larsen, B. A. (2015). Electric field structures and waves at plasma boundaries in the inner magnetosphere. *Journal of Geophysical Research: Space Physics*, 120(6), 4246–4263. https://doi.org/10.1002/ 2015ia021137
- Mauk, B. H. (1986). Quantitative modeling of the 'convection surge' mechanism of ion acceleration. *Journal of Geophysical Research*, 91(A12), 13423–13431. https://doi.org/10.1029/JA091iA12p13423
- Mauk, B. H., Fox, N. J., Kanekal, S. G., Kessel, R. L., Sibeck, D. G., & Ukhorskiy, A. (2012). Science objectives and rationale for the radiation belt storm probes mission. *Space Science Reviews*, 179(1–4), 3–27. https://doi.org/10.1007/s11214-012-9908-y
- Mauk, B. H., & Mcilwain, C. E. (1974). Correlation of Kp with substorm-injected plasma boundary. *Journal of Geophysical Research*, 79(22), 3193–3196. https://doi.org/10.1029/Ja079i022p03193
- McIlwain, C. E. (1974). Substorm injection boundaries. In B. M. McCormac (Ed.), Magnetospheric physics (pp. 143-154). Springer.
- Mitani, T., Takashima, T., Kasahara, S., Miyake, W., & Hirahara, M. (2018). High-energy electron experiments (HEP) aboard the ERG (Arase) satellite. Earth Planets and Space, 70(1), 77. https://doi.org/10.1186/s40623-018-0853-1
- Miyoshi, Y., Hori, T., Shoji, M., Teramoto, M., Chang, T. F., Segawa, T., et al. (2018). The ERG science center. Earth Planets and Space, 70(1), 96. https://doi.org/10.1186/s40623-018-0867-8
- Miyoshi, Y., Shinohara, I., Takashima, T., Asamura, K., Higashio, N., Mitani, T., et al. (2018). Geospace exploration project ERG. Earth Planets and Space, 70(1), 101. https://doi.org/10.1186/s40623-018-0862-0
- Motoba, T., Ohtani, S., Claudepierre, S. G., Reeves, G. D., Ukhorskiy, A. Y., & Lanzerotti, L. J. (2020). Dynamic properties of particle injections inside geosynchronous orbit: A multisatellite case study. *Journal of Geophysical Research: Space Physics*, 125(9), e2020JA028215. https://doi.org/10.1029/2020JA028215
- Mourenas, D., & Ripoll, J. F. (2012). Analytical estimates of quasi-linear diffusion coefficients and electron lifetimes in the inner radiation belt. *Journal of Geophysical Research*, 117(A1). https://doi.org/10.1029/2011ja016985
- Nakamura, R., Baker, D. N., Yamamoto, T., Belian, R. D., Bering, I. E. A., Benbrook, J. R., & Theall, J. T. (1994). Particle and field signatures during pseudobreakup and major expanson onset. *Journal of Geophysical Research*, 99(A1), 207–221. https://doi.org/10.1029/93JA02207
- Ni, B., Summers, D., Xiang, Z., Dou, X., Tsurutani, B. T., Meredith, N. P., et al. (2023). Unique banded structures of plasmaspheric hiss waves in the Earth's magnetosphere. *Journal of Geophysical Research: Space Physics*, 128(3), e2023JA031325. https://doi.org/10.1029/2023ja031325
 Nosé, M., Koshiishi, H., Matsumoto, H., C, P., Brandt, S., Keika, K., et al. (2010). Magnetic field dipolarization in the deep inner magnetosphere
- and its role in development of O⁺-rich ring current. *Journal of Geophysical Research*, 115(A9). https://doi.org/10.1029/2010ja015321
 Ohtani, S., Korth, H., Brandt, P. C., Blomberg, L. G., Singer, H. J., Henderson, M. G., et al. (2007). Cluster observations in the inner magnetosphere during the 18 April 2002 sawtooth event: Dipolarization and injection at R = 4.6 R_E. *Journal of Geophysical Research*, 112(A8).
- https://doi.org/10.1029/2007ja012357

 Olson, W. P., & Pfitzer, K. A. (1974). A quantitative model of the magnetospheric magnetic field. *Journal of Geophysical Research*, 79(25), 3739–3748. https://doi.org/10.1029/JA079i025p03739
- Papitashvili, N. E., & King, J. H. (2020). OMNI hourly data set [Dataset]. NASA Space Physics Data Facility. https://doi.org/10.48322/1shr-ht18 Pulkkinen, T. I. (1996). Pseudobreakup or substorm? In Substorms 3, ESA SP-339 (pp. 285–293).

REEVES ET AL. 15 of 16

- Quinn, J. M., & Southwood, D. J. (1982). Observations of parallel ion energization in the equatorial region. *Journal of Geophysical Research*, 87(A12), 10536–10540. https://doi.org/10.1029/JA087iA12p10536
- Reeves, G. D. (1998). Relativistic electrons and magnetic storms: 1992–1995. Geophysical Research Letters, 25(11), 1817–1820. https://doi.org/10.1029/98g101398
- Reeves, G. D. (2025). Data for multi-Platform observations of the radial penetration of substorm injected electrons and subsequent slot-filling event [Dataset]. Zenodo. https://doi.org/10.5281/zenodo.15285033
- Reeves, G. D., Belian, R. D., Cayton, T. C., Henderson, M. G., Christensen, R. A., McLachlan, P. S., & Ingraham, J. C. (1996). Los Alamos geosynchronous space weather data for radiation belt modeling. In J. F. Lemaire, D. Heyndrickx, & D. N. Baker (Eds.), Radiation belts: Models and standards (pp. 237–240). American Geophysical Union.
- Reeves, G. D., Belian, R. D., & Fritz, T. A. (1991). Numerical tracing of energetic particle drifts in a model magnetosphere. *Journal of Geophysical Research*, 96(A8), 13997–14008. https://doi.org/10.1029/91JA01161
- Reeves, G. D., Friedel, R. H., Larsen, B. A., Skoug, R. M., Funsten, H. O., Claudepierre, S. G., et al. (2016). Energy-dependent dynamics of keV to MeV electrons in the inner zone, outer zone, and slot regions. *Journal of Geophysical Research: Space Physics*, 121(1), 397–412. https://doi.org/10.1002/2015JA021569
- Reeves, G. D., Friedel, R. W. H., Henderson, M. G., Korth, A., McLachlan, P. S., & Belian, R. D. (1996). Radial propagation of substorm injections. In *Proceedings of the 3rd international conference on substorms*.
- Reeves, G. D., & Henderson, M. G. (2001). The storm-substorm relationship: Ion injections in geosynchronous measurements and composite energetic neutral atom images. *Journal of Geophysical Research*, 106(A4), 5833–5844. https://doi.org/10.1029/2000ja003017
- Reeves, G. D., Henderson, M. G., Skoug, R. M., Thomsen, M. F., Borovsky, J. E., Funsten, H. O., et al. (2003). IMAGE, POLAR, and geosynchronous observations of substorm and ring current ion injection. In A. S. Sharma, Y. Kamide, & G. S. Lakhina (Eds.), *Disturbances in geospace: The storm-substorm relationship* (pp. 91–101). AGU.
- Ripoll, J. F., Loridan, V., Denton, M. H., Cunningham, G., Reeves, G., Santolík, O., et al. (2019). Observations and fokker-planck simulations of the L-shell, energy, and pitch angle structure of Earth's electron radiation belts during quiet times. *Journal of Geophysical Research: Space Physics*, 124(2), 1125–1142. https://doi.org/10.1029/2018ja026111
- Ripoll, J. F., Reeves, G. D., Cunningham, G. S., Loridan, V., Denton, M., Santolík, O., et al. (2016). Reproducing the observed energy-dependent structure of Earth's electron radiation belts during storm recovery with an event-specific diffusion model. *Geophysical Research Letters*, 43(11), 5616–5625. https://doi.org/10.1002/2016g1068869
- Ripoll, J. F., Thaller, S. A., Hartley, D. P., Cunningham, G. S., Pierrard, V., Kurth, W. S., et al. (2022). Statistics and empirical models of the plasmasphere boundaries from the Van Allen probes for radiation belt physics. *Geophysical Research Letters*, 49(21), e2022GL101402. https:// doi.org/10.1029/2022g1101402
- Roederer, J. G. (1967). On the adiabatic motion of energetic particles in a model magnetosphere. *Journal of Geophysical Research*, 72(3), 981–992. https://doi.org/10.1029/JZ072i003p00981
- Sergeev, V. A., Shukhtina, M. A., Rasinkangas, R., Korth, A., Reeves, G. D., Singer, H. J., et al. (1998). Event study of deep energetic particle injections during substorm. *Journal of Geophysical Research*, 103(A5), 9217–9234. https://doi.org/10.1029/97ja03686
- Shprits, Y. Y., Thorne, R. M., Reeves, G. D., & Friedel, R. (2005). Radial diffusion modeling with empirical lifetimes: Comparison with CRRES observations. *Annales Geophysicae*, 23(4), 1467–1471. https://doi.org/10.5194/angeo-23-1467-2005
- Smith, E. J., & Wolfe, J. H. (2012). Observations of interaction regions and corotating shocks between one and five AU: Pioneers 10 and 11. Geophysical Research Letters, 3(3), 137–140. https://doi.org/10.1029/GL003i003p00137
- Sorathia, K. A., Michael, A., Merkin, V. G., Ukhorskiy, A. Y., Turner, D. L., Lyon, J. G., et al. (2021). The role of mesoscale plasma sheet dynamics in ring current formation. Frontiers in Astronomy and Space Sciences, 8, 761875. https://doi.org/10.3389/fspas.2021.761875
- Spanswick, E., Wallis, D., Donovan, E., & Jackel, B. (2025). NORSTAR single frequency single beam riometers dataset [Dataset]. University of Calgary. https://doi.org/10.11575/AFYX-M516
- Turner, D. L., Claudepierre, S. G., Fennell, J. F., O'Brien, T. P., Blake, J. B., Lemon, C., et al. (2015). Energetic electron injections deep into the inner magnetosphere associated with substorm activity. *Geophysical Research Letters*, 42(7), 2079–2087. https://doi.org/10.1002/2015gl063225
- Turner, D. L., Fennell, J. F., Blake, J. B., Claudepierre, S. G., Clemmons, J. H., Jaynes, A. N., et al. (2017). Multipoint observations of energetic particle injections and substorm activity during a conjunction between magnetospheric multiscale (MMS) and Van Allen probes. *Journal of Geophysical Research: Space Physics*, 122(11), 11481–11504, https://doi.org/10.1002/2017ja024554
- Wolf, R. A., Kumar, V., Toffoletto, F. R., Erickson, G. M., Savoie, A. M., Chen, C. X., & Lemon, C. L. (2006). Estimating local plasma sheet PV^{5/3} from single-spacecraft measurements. *Journal of Geophysical Research*, 111(A12). https://doi.org/10.1029/2006ja012010
- Wolf, R. A., Wan, Y., Xing, X., Zhang, J. C., & Sazykin, S. (2009). Entropy and plasma sheet transport. *Journal of Geophysical Research*, 114(A9). https://doi.org/10.1029/2009ja014044

References From the Supporting Information

- Hosokawa, K., Oyama, S. I., Ogawa, Y., Miyoshi, Y., Kurita, S., Teramoto, M., et al. (2023). A ground-based instrument suite for integrated high-time resolution measurements of pulsating Aurora with arase. *Journal of Geophysical Research: Space Physics*, 128(8), e2023JA031527. https://doi.org/10.1029/2023ja031527
- Reeves, G. D., Fritz, T. A., Cayton, T. E., & Belian, R. D. (1990). Multi-satellite measurements of the substorm injection region. *Geophysical Research Letters*, 17(11), 2015–2018. https://doi.org/10.1029/GL017i011p02015

REEVES ET AL. 16 of 16